Crystal Structure of Human Prostaglandin F Synthase (AKR1C3)[†,‡]

Junichi Komoto,[§] Taro Yamada,[§] Kikuko Watanabe,[||] and Fusao Takusagawa*[,§]

Department of Molecular Biosciences, University of Kansas, 1200 Sunnyside Avenue, Lawrence, Kansas 66045-7534, and Division of Applied Life Science, Graduate School of Integrated Science and Art, University of East Asia, 2-1 Ichinomiya-gakuencho, Shimonoseki, Yamaguchi 751-0807, Japan

Received November 15, 2003; Revised Manuscript Received December 24, 2003

ABSTRACT: Prostaglandin H_2 (PGH_2) formed from arachidonic acid is an unstable intermediate and is efficiently converted into more stable arachidonate metabolites (PGD_2, PGE_2, and PGF_2) by the action of three groups of enzymes. Prostaglandin F synthase (PGFS) was first purified from bovine lung and catalyzes the formation of 9α,11β-PGF_2 from PGD_2 and $PGF_{2\alpha}$ from PGH_2 in the presence of NADPH. Human PGFS is 3α-hydroxysteroid dehydrogenase (3α-HSD) type II and has PGFS activity and 3α-HSD activity. Human lung PGFS has been crystallized with the cofactor $NADP^+$ and the substrate PGD_2, and with the cofactor NADPH and the inhibitor rutin. These complex structures have been determined at 1.69 Å resolution. PGFS has an $(\alpha/\beta)_8$ barrel structure. The cofactor and substrate or inhibitor bind in a cavity at the C-terminal end of the barrel. The cofactor binds deeply in the cavity and has extensive interactions with PGFS through hydrogen bonds, whereas the substrate (PGD_2) is located above the bound cofactor and has little interaction with PGFS. Despite being largely structurally different from PGD_2, rutin is located at the same site of PGD_2, and its catechol and rhamnose moieties are involved in hydrogen bonds with PGFS. The catalytic site of PGFS contains the conserved Y55 and H117 residues. The carbonyl O_{11} of PGD_2 and the hydroxyl O_{13} of rutin are involved in hydrogen bonds with Y55 and H117. The cyclopentane ring of PGD_2 and the phenyl ring of rutin face the *re*-side of the nicotinamide ring of the cofactor. On the basis of the catalytic geometry, a direct hydride transfer from NADPH to PGD_2 would be a reasonable catalytic mechanism. The hydride transfer is facilitated by protonation of carbonyl O_{11} of PGD_2 from either H117 (at low pH) or Y55 (at high pH). Since the substrate binding cavity of PGFS is relatively large in comparison with those of AKR1C1 and AKR1C2, PGFS (AKR1C3) could catalyze the reduction and/or oxidation reactions of various compounds over a relatively wide pH range.

Prostaglandins (PGs) are ubiquitously distributed in virtually all mammalian tissues and organs and have numerous and diverse biological effects on a variety of physiological and pathological activities such as smooth muscle contraction, inflammation, and blood clotting. In humans, the most important prostaglandin precursor is arachidonic acid, a C_{20} polyunsaturated fatty acid that has nonconjugated double bonds. PGs synthesized from arachidonic acid have the subscript 2 (the "series-2" PGs), such as PGD_2,[1] PGF_2, and PGH_2. PGH_2 is an unstable intermediate formed from PGG_2 by the action of PGH_2 hydroperoxidase in the arachidonate cascade. In mammalian systems, PGH_2 is efficiently converted into more stable arachidonate metabolites, such as PGD_2, PGE_2, and PGF_2, by the action of three groups of enzymes (*1*).

F series PGs are widely distributed in various organs of mammals (*2*, *3*) and exhibit a variety of biological activities, including contraction of pulmonary arteries (*4*−*7*). Three different biosynthetic pathways have been described for the formation of PGF_2: synthesis from PGD_2 by PGD_2 11-ketoreductase (*8*, *9*), from PGE_2 by PGE_2 9-ketoreductase (*10*, *11*), and from PGH_2 by PGH_2 9,11-endoperoxide reductase (*12*−*15*).

PGFS (EC 1.1.1.188) was first purified from bovine lung (*15*). It catalyzes the formation of 9α,11β-PGF_2 from PGD_2 (PGD_2 11-ketoreductase activity) in the presence of NADPH (*16*) as shown Figure 1A. It has been reported that this enzyme also catalyzes the formation of $PGF_{2\alpha}$ from PGH_2 (PGH_2 9,11-endoperoxide reductase activity). However, this enzyme does not catalyze the reduction of PGE_2 (*16*). Interestingly, this enzyme exhibits reductase activities toward

[†] This work has been supported by Grant GM37233 (F.T.) from the National Institutes of Health. Use of the Argonne National Laboratory Structural Biology Center beamline at the Advanced Photon Source was supported by the U.S. Department of Energy, Office of Energy Research, under contract W-31-109-ENG-38.

[‡] The atomic coordinates and structure factors have been deposited with the Brookhaven Protein Data Bank as entries 1RY0 and 1RY8.

* To whom correspondence should be addressed: Department of Molecular Biosciences, 3004 Haworth Hall, University of Kansas, 1200 Sunnyside Ave., Lawrence, KS 66045-7534. Telephone: (785) 864-4727. E-mail: xraymain@ku.edu.

[§] University of Kansas.

[||] University of East Asia.

[1] Abbreviations: 9α,11β-PGF_2, 9α,11β-prostaglandin F_2; PQ, 9,10-phenanthrene quinone; AKR, aldo-keto reductase; AKR1C1, human 20α(3α)-HSD; AKR1C1−($NADP^+$+progesterone), $NADP^+$- and progesterone-bound AKR1C1; AKR1C2, human type III 3α-HSD/bile acid binding protein; AKR1C2−($NADP^+$+ursodeoxycholate), $NADP^+$- and ursodeoxycholate-bound AKR1C2; AKR1C3, human type II 3α-HSD; HSD, hydroxysteroid dehydrogenase; PGD_2, prostaglandin D_2; $PGF_{2\alpha}$, 9α,11α-prostaglandin F_2; PGFS, prostaglandin F synthase; PGFS−($NAPH^+$+PGD_2), $NADP^+$- and PGD_2-bound PGFS; PGFS−(NADPH +rutin), NADPH- and rutin-bound PGFS; PGG_2, prostaglandin G_2; PGH_2, prostaglandin H_2.

10.1021/bi036046x CCC: $27.50
Published on Web 02/07/2004

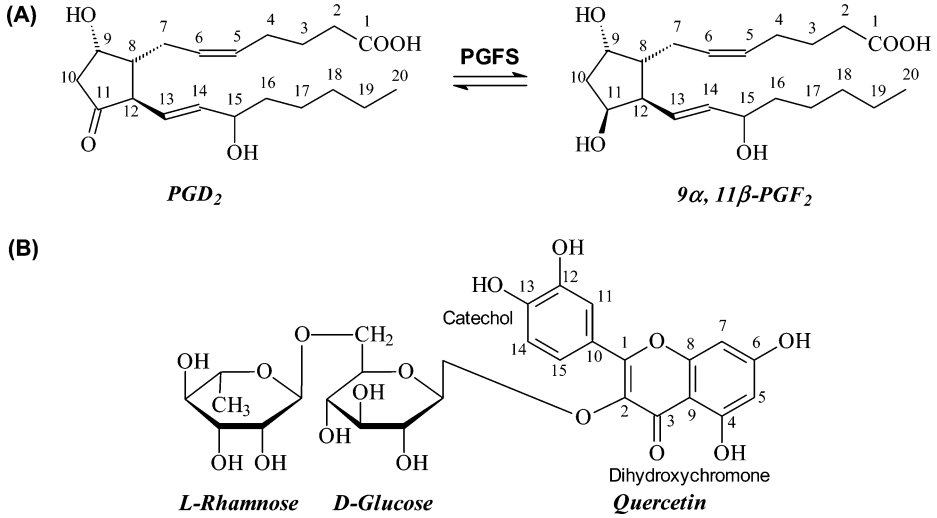

FIGURE 1: Chemical formulas of (A) PGD_2 and 9α,11β-PGF_2 and (B) rutin.

various carbonyl compounds, such as 9,10-phenanthrene quinone (PQ), nitrobenzaldehyde, and nitroacetophenone (*16*). Although the PGD_2 11-ketoreductase activity is competitively inhibited by PQ, PGH_2 9,11-endoperoxide reductase activity is not inhibited by PGD_2 or PQ (*15*). PGFS belongs to the aldo-keto hydroxysteroid reductase family based on substrate specificity, molecular weight, and amino acid sequence (*17*, *18*).

In human liver, 3α-HSD with dihydrodiol dehydrogenase activity exists in multiple forms (*19*, *20*), and four types of cDNAs for the enzymes have been cloned (*21*−*24*). The 3α-HSD isoforms have sequences that are 83−98% identical, belong to the AKR superfamily, and have been systematically named AKR1C1−AKR1C4 (*25*). AKR1C3 has been designated as 3α-HSD type 2 (*24*). A cDNA (GenBank entry D17793) that is more than 99% homologous with AKR1C3 cDNA has been cloned from human myeloblasts (*26*). Although this enzyme differs in two amino acid at positions 75 (Lys vs Met) and 175 (Met vs Glu) from the original AKR1C3, the catalytic property is exactly the same (*26*). Furthermore, this new enzyme and the original AKR1C3 have not only the AKR1C3 activity but also the PGD_2 11-ketoreductase activity found in the bovine lung and liver (*26*). It was found that this enzyme has the same amino acid sequence as PGFS isolated from human lung by using cDNA of bovine lung-type PGFS as a probe (*27*). The NIH Mammalian Gene Collection Program Team has confirmed that PGFS is AKR1C3 (*28*). Human lung PGFS catalyzes the reduction ($PGD_2 \rightarrow$ 9α,11β-PGF_2) at low pH and the oxidation (9α,11β-$PGF_2 \rightarrow PGD_2$) at high pH (*26*, *27*). The product, 9α,11β-PGF_2, has been reported to exhibit various biological activities (*29*−*32*), and its levels are increased in bronchoalveolar lavage fluid, plasma, and urine in patients with mastocytosis (*29*) and bronchial asthma (*33*−*35*).

Rutin shown in Figure 1B is one of the most commonly found flavonol glycosides identified as vitamin P with quercetin and hesperidin and is widely present in many plants, especially the buckwheat plant. Rutin has been reported to have clinically relevant functions. It was established that rutin antagonizes the increase in capillary fragility associated with hemorrhagic diseases, reduces high blood pressure (*36*, *37*), decreases the permeability of vessels, has an antiedema effect, reduces the risk of arteriosclerosis (*38*), and exhibits antioxidant activity (*39*). Quercitrin (a part of rutin) exhibits antibacterial effects and protects against naftodianthron phototoxicity (*40*, *41*). Rutin is also known as an AKR inhibitor (*42*−*44*). Indeed, rutin inhibits bovine PGFS activity by 50% (IC_{50}) at 70 μM (*45*). However, the mechanism of inhibition is unknown.

Here we report crystal structures of human lung PGFS ternary complexes, PGFS−($NADP^+$+PGD_2) and PGFS−(NADPH+rutin). On the basis of the structures, we propose a detailed catalytic mechanism of PGFS and an inhibitory mechanism of rutin, and describe the similarities and differences among PGFS (AKR1C3), AKR1C1, and AKR1C2.

EXPERIMENTAL PROCEDURES

Crystallization. Human lung PGFS was purified from *Escherichia coli* HB101 harboring the pUC-hLuFS plasmids encoding the human lung PGFS sequences. The enzyme was purified to electrophoretic homogeneity using methods previously described (*27*). The hanging drop method of vapor diffusion was employed for crystallization of the enzymes. PGD_2 and rutin were dissolved in DMSO and added to the crystallization solution. Thick plate-shaped crystals of PGFS−($NADP^+$+PGD_2) and PGFS−(NADPH+rutin) suitable for X-ray diffraction studies were grown in a solution containing 1.4 mM PGD_2 or rutin, 1.2 mM $NADP^+$ and NADPH, 50 mM MES buffer (pH 6.0), and 25% (w/v) PEG 8000 with a protein concentration of 20 mg/mL at 4 °C. The crystals were grown for 2−3 days. The crystals of PGFS−(NADPH+rutin) were yellowish, whereas those of PGFS−($NADP^+$+PGD_2) were colorless.

Data Measurement. Diffraction data were collected from cryocooled crystals on beamline 19BM at the Advanced Photon Source (APS) of the Argonne National Laboratory (Argonne, IL). The crystals (~0.3 mm × 0.2 mm × 0.1 mm) diffract up to 1.6 Å, and five data sets of PGFS−($NADP^+$+PGD_2) and three data sets of PGFS−(NADPH +rutin) were collected at 1.69 Å resolution. The data were processed with the program DENZO/SCALEPACK (*46*), and averaged to obtain one complete data set of PGFS−($NADP^+$+PGD_2) and one complete data set of PGFS−(NADPH+rutin). Data statistics are given in Table 1.

Crystal Structure Determination. The deduced unit cell dimensions of PGFS−($NANP^+$+PGD_2) and PGFS−

Table 1: Crystallographic Statistics[a]

	PGFS−(NADP$^+$+PGD$_2$)	PGSF−(NADPH+rutin)
unit cell	a = 46.97 Å, b = 49.18 Å, c = 83.52 Å, α = 73.8°, β = 85.9°, γ = 69.8°	a = 47.06 Å, b = 49.37 Å, c = 83.59 Å, α = 73.9°, β = 86.3°, γ = 69.9°
resolution (Å)	1.69	1.69
total no. of observations	345615	213639
no. of unique reflections	74430	72690
completeness (%)	95.8 (75.1)	92.9 (90.2)
R_{sym} (%) (outer shell)[b,c]	0.035 (0.183)	0.030 (0.158)
no. of protein non-hydrogen atoms	5126	5126
cofactor	2 NADP$^+$	2 NADPH
substrate/inhibitor	∼1 PGD$_2$	2 rutin
no. of solvent molecules (H_2O)	384	507
resolution range (Å)	10−1.69	10−1.69
total no. of reflections used in R_{cryst}	66283	65156
total no. of reflections used in R_{free}	7365	7240
R_{cryst} (outer shell)[c,d]	0.208 (0.375)	0.205 (0.367)
R_{free} (outer shell)[c]	0.248 (0.396)	0.249 (0.400)
rmsd for bond distances (Å)	0.006	0.007
rmsd for bond angles (deg)	1.2	1.2
rmsd for torsion angles (deg)	25.8	25.0
most favored region (%) of the Ramachandran plot	90.4	91.6
additional allowed region (%) of the Ramachandran plot	9.3	7.9

[a] Space group $P1$; M_r of subunit of 35 530; two complexes in the unit cell; V_M = 2.45 Å^3; 50% solvent content. [b] $R_{sym} = \sum_h\sum_i|I_{hi} - \langle I_h\rangle|/\sum_h\sum_i|I_{hi}|$. [c] Outer shell of 1.69−1.77 Å resolution. [d] $R_{cryst} = \sum|F_o - F_c|/\sum|F_o|$.

(NADPH+rutin) indicate that these crystals are isomorphous with respect to each other. The unit cell dimensions and space group ($P1$) indicate that the unit cell contains two complexes. The crystal structure of the PGFS−(NADP$^+$+PGD$_2$) complex was initially determined by a molecular replacement procedure using a poly-Ser model of 3α-HSD type 3 (PDB entry 1AFS). The side chains of the polypeptide chain were built in $2F_o - F_c$ maps. The model was refined by the simulated annealing procedures of X-PLOR (*47*). The $2F_o - F_c$ and $F_o - F_c$ maps showed two large significant residual electron density peaks in each active site (Figure 2). A NADP$^+$ molecule was built in one of the residual electron density peaks. The other residual electron density peak was relatively weak and assigned to PGD$_2$. The PGD$_2$ molecule has an approximately 2-fold symmetry (i.e., a cyclopentane ring head and two tails), so a PGD$_2$ molecule was fitted into the residual electron density in two ways (i.e., either the hydroxyl O_9 or the carbonyl O_{11} enters the catalytic site). Both models were refined with the simulated annealing procedures of X-PLOR. The R and R_{free} values of both models were the same, indicating that it is impossible to determine the orientation of the PGD$_2$ molecule by this X-ray study. On the basis of the catalytic reaction, the model with the carbonyl O_{11} entering the catalytic site was selected as the correct orientation model. Since the temperature factors of PGD$_2$ were much higher than those of the protein, the occupancy factors were set to 0.5. Other well-defined residual peaks were assigned to water molecules. Water molecules having temperature factors higher than 25 Å^2 had their occupancy factors reduced until their temperature factors were ∼25 Å^2. Water molecules with occupancy factors higher than 0.33 were included in the final refinement. Two complexes were refined independently with all data (no σ cutoff) at 1.69 Å resolution.

Since the crystal of PGFS−(NADPH+rutin) had a yellowish color, a rutin molecule-bound PGFS was expected. The $2F_o - F_c$ and $F_o - F_c$ maps showed two well-defined residual electron density peaks corresponding to NADPH and rutin. The NADPH was at the NADP$^+$ binding site seen in the PGFS−(NADP$^+$+PGD$_2$) structure. A well-defined residual electron density peak corresponding to rutin showed clearly the shape and orientation of a rutin molecule. NADPH and rutin were fitted into the residual electron density peaks, and the complex structure was refined with the same procedure applied to the PGFS−(NADP$^+$+PGD$_2$) structure.

RESULTS

Overall Structure. The crystallographic refinement parameters (Table 1), final $2F_o - F_c$ maps, and conformational analysis by PROCHECK (*48*) indicate that the crystal structures of the PGFS−(NADP$^+$+PGD$_2$) and PGFS−(NADPH+rutin) complexes have been determined successfully. The two complexes are isomorphous with respect to each other. Each crystal structure contains two independent PGFS complexes in the unit cell, but there is neither specific symmetry nor strong interaction between the two complexes in each unit cell. The two complexes are nearly identical with a maximum rmsd of 0.35 Å.

As shown in Figure 3, the protein structure of PGFS displays the characteristic fold of the AKR superfamily (*49*), an $(\alpha/\beta)_8$ barrel with three associated large loops (Figure 3). The β-strands ($\beta1-\beta8$) form the cylindrical core of the barrel and are surrounded by α-helices (α1−α8), while the accompanying loops (loop 4, loop 7, and loop 9) partially cover the C-terminal end of the barrel. In addition to the $(\alpha/\beta)_8$ core structure, there are two β-strands (B1 and B2) from the N-terminus sealing the N-terminal end of the barrel and two α-helices (H1 and H2) from the C-terminal part of the molecule packed by the side of the barrel. These additional β-strands and α-helices are conserved in other AKR structures (*49*). The topology of the polypeptide is ∼B1(7−9)-B2(15−17)-β1(19−22)-(loop 1)-α1(32−44)-β2-(48−50)-(loop 2)-α2(58−70)-β3(80−85)-(loop 3)-α3(92−106)-β4(113−116)-(loop 4)-α4(144−156)-β5(162−166)-

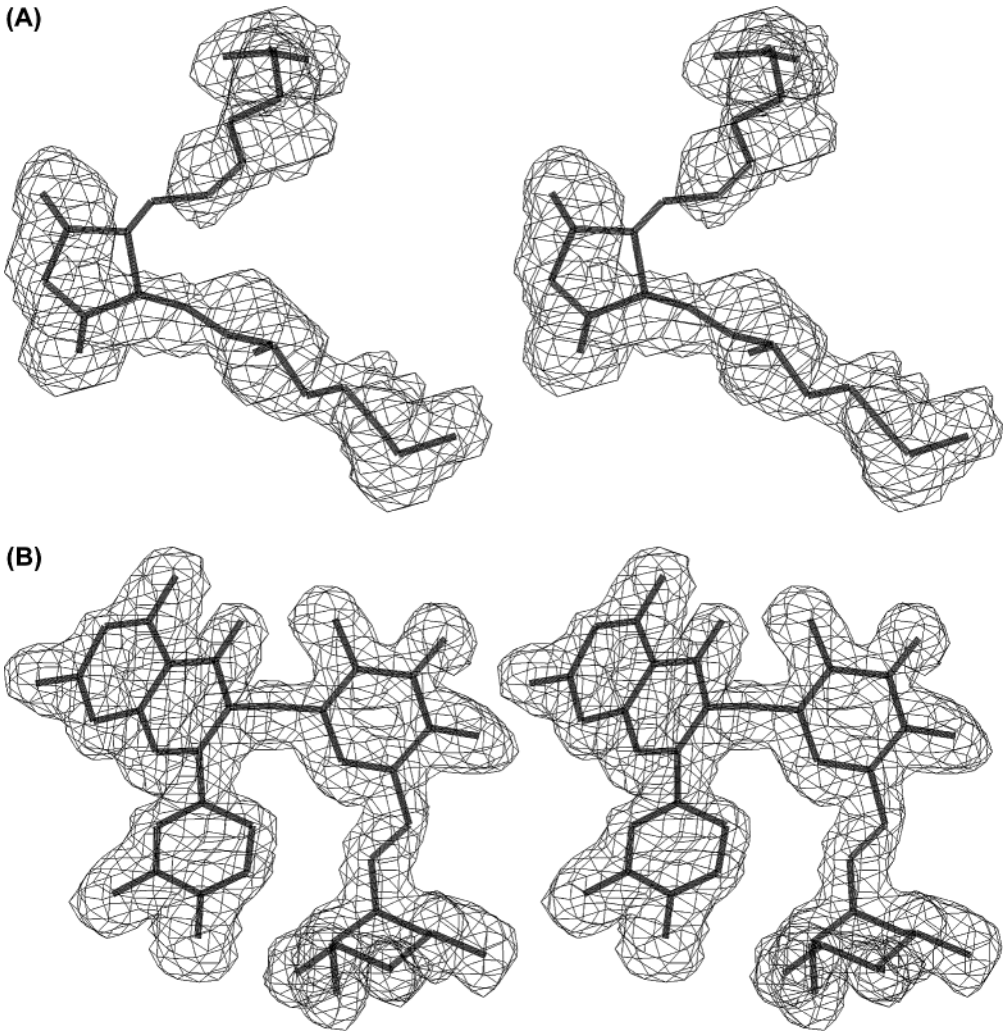

FIGURE 2: Final $2F_o - F_c$ maps showing electron density peaks of PGD_2 and rutin: (A) slightly disordered PGD_2 at a contour level of 1σ and (B) well-defined rutin at a contour level 1.25σ.

(loop 5)-α5(170−177)-*β*6(188−192)-(loop 6)-α6(200−208)-*β*7(212−216)-(loop 7)-α7(239−248)-H1(252−262)-*β*8(266−270)-(loop 8)-α8(274−284)-H2(290−297)-(loop 9). The cofactor and substrate or inhibitor bind in a cavity at the C-terminal end of the barrel.

Cofactor (NADP$^+$ or NADPH) in the Active Site. Figure 4 shows the possible hydrogen bonds between the cofactor and PGFS. Since both $NADP^+$ in PGFS−($NADP^+$+PGD_2) and NADPH in PGFS−(NADPH+rutin) bind the same site and have the same hydrogen bonding scheme, "NADP" represents both $NADP^+$ and NADPH in this paper. NADP is located in a deep cavity at the C-terminal end of the barrel and extends across the barrel closer to the core. The bound NADP interacts with amino acid residues in the loops connecting *β*-strands and α-helices. The nicotinamide moiety is located within the enzyme near the center of the barrel, while the adenine moiety is exposed on the outer surface of the protein. The adenine ring interacts with Q279 and N280 in helix α8 and a water (W_{231}). The phosphate attached to $O_{2'}$ of adenosine is heavily involved in hydrogen bonding with L270, S271, Y272, and R276 in loop 8. The diphosphate group participates in hydrogen bonds with S217, L219, S221, and Q222 in loop 7 and K270 in loop 8. The ribose $O_{2'}$ and $O_{3'}$ of the nicotinamide nucleotide moiety is involved in hydrogen bonds with Y24 in loop 1 and D50 in loop 2, respectively. The nicotinamide ring is recognized by three hydrogen bonds with S166 and N167 in loop 5 and Q190 in loop 6 and a stacking interaction with the phenyl ring of Y216 in loop 7. The characteristic "safety-belt" hydrogen bond (*50*−*52*) over the bound NADP is seen between Q222 and K270.

PGD_2 in the Active Site. As shown in Figure 1, PGD_2 is composed of a head (cyclopentane ring) and two tails. The X-ray refinement suggested that the occupancy of PGD_2 in the PGFS complex is less than 50%, and $2F_o - F_c$ maps showed some disorder in the two tail sections (Figure 2A). A PGD_2 is located above the bound $NADP^+$ and is surrounded by loops 1, 2, 4, 7, and 9. The cyclopentane ring (head) is deep within the active site cavity, whereas the two tail sections are far from the active site and interact little with PGFS. As shown in Figure 5A, the carbonyl O_{11} participates in hydrogen bonds with O_H[Y55] and N_{E2}[H117]. N_{D1} of H117 is involved in a hydrogen bond with a water in a water channel, while O_H of Y55 participates in a hydrogen bonding chain (N_{E2}[H117]···O_{11}[PGD_2]···O_H[Y55]···N_Z-[K84]···O_{D1}[D50]). The cyclopentane ring is nearly parallel to the nicotinamide ring of $NADP^+$ and faces the *re*-side of the ring. The distance between C_{11} of PGD_2 and C_4 of $NADP^+$ is 3.6 Å, suggesting that the *pro-R* H_4 can be directly transferred from NADPH to C_{11} of PGD_2 to produce 9α,-11*β*-PGF_2. Neither the hydroxyl groups (O_9 and O_{15}) nor the carboxyl group (C_1) is involved in hydrogen bonding

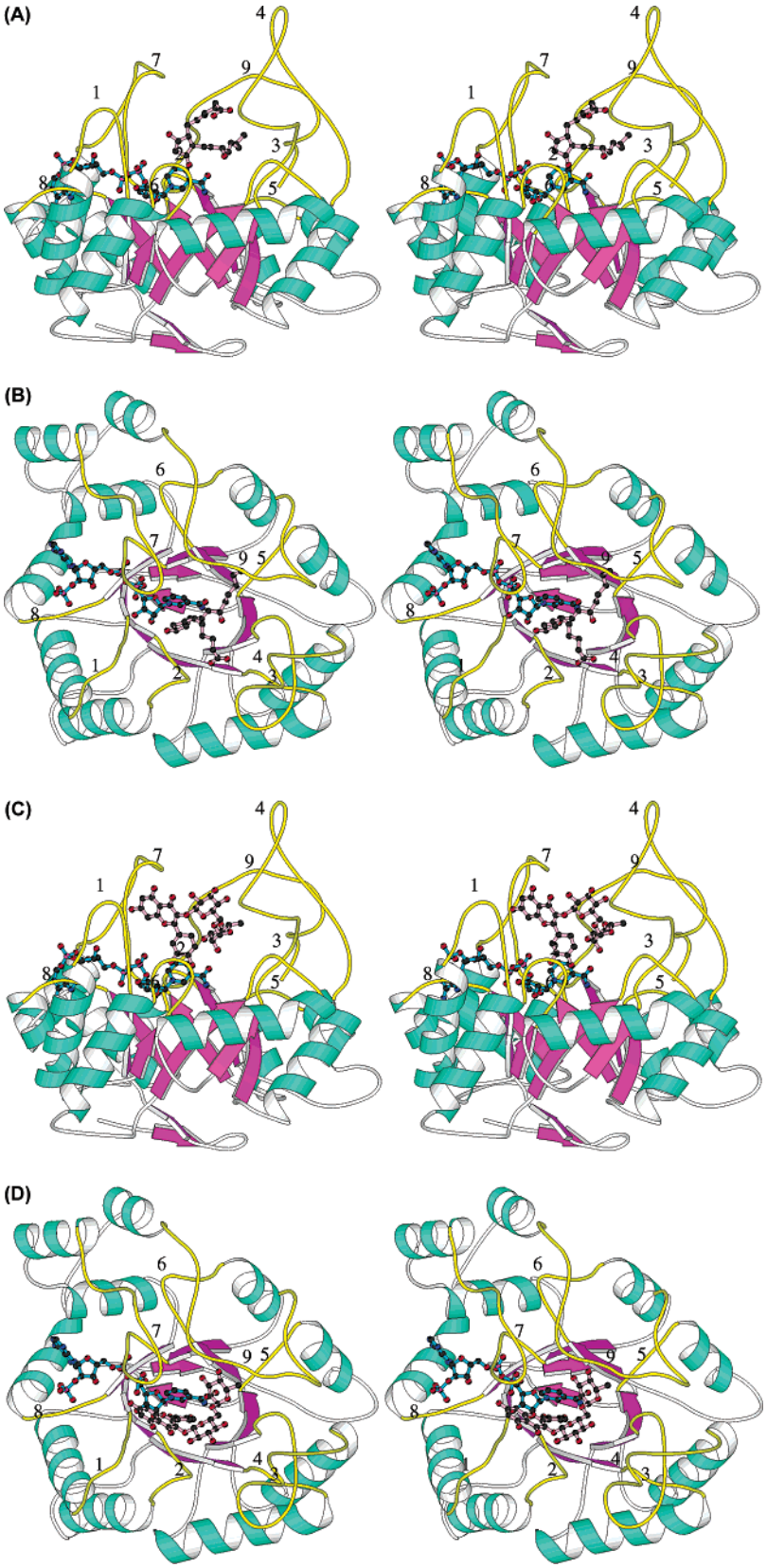

FIGURE 3: Ribbon drawings of the PGFS complexes: (A) side view of PGFS−(NADP$^+$+PGD$_2$), (B) top view of PGFS−(NADP$^+$+PGD$_2$), (C) side view of PGFS−(NADPH+rutin), and (D) top view of PGFS−(NADPH+rutin). The α-helices and β-strands in the α/β base are colored aquamarine and magenta, respectively. The loops are shown in yellow and labeled with numbers. The bound NADP$^+$/NADPH and PGD$_2$/rutin are colored cyan and light pink, respectively.

with PGFS. Unlike that with the bound NADP$^+$, there is little polar interaction between PGD$_2$ and PGFS.

Rutin in the Active Site. As shown in Figure 1, rutin is composed of quercetin (catechol and dihydroxychromone), D-glucose, and L-rhamnose, and is a relatively large molecule compared to PGD$_2$. A well-defined rutin molecule is found in the active site of PGFS (Figure 2B). A rutin molecule sits in a relatively large hydrophobic pocket composed of

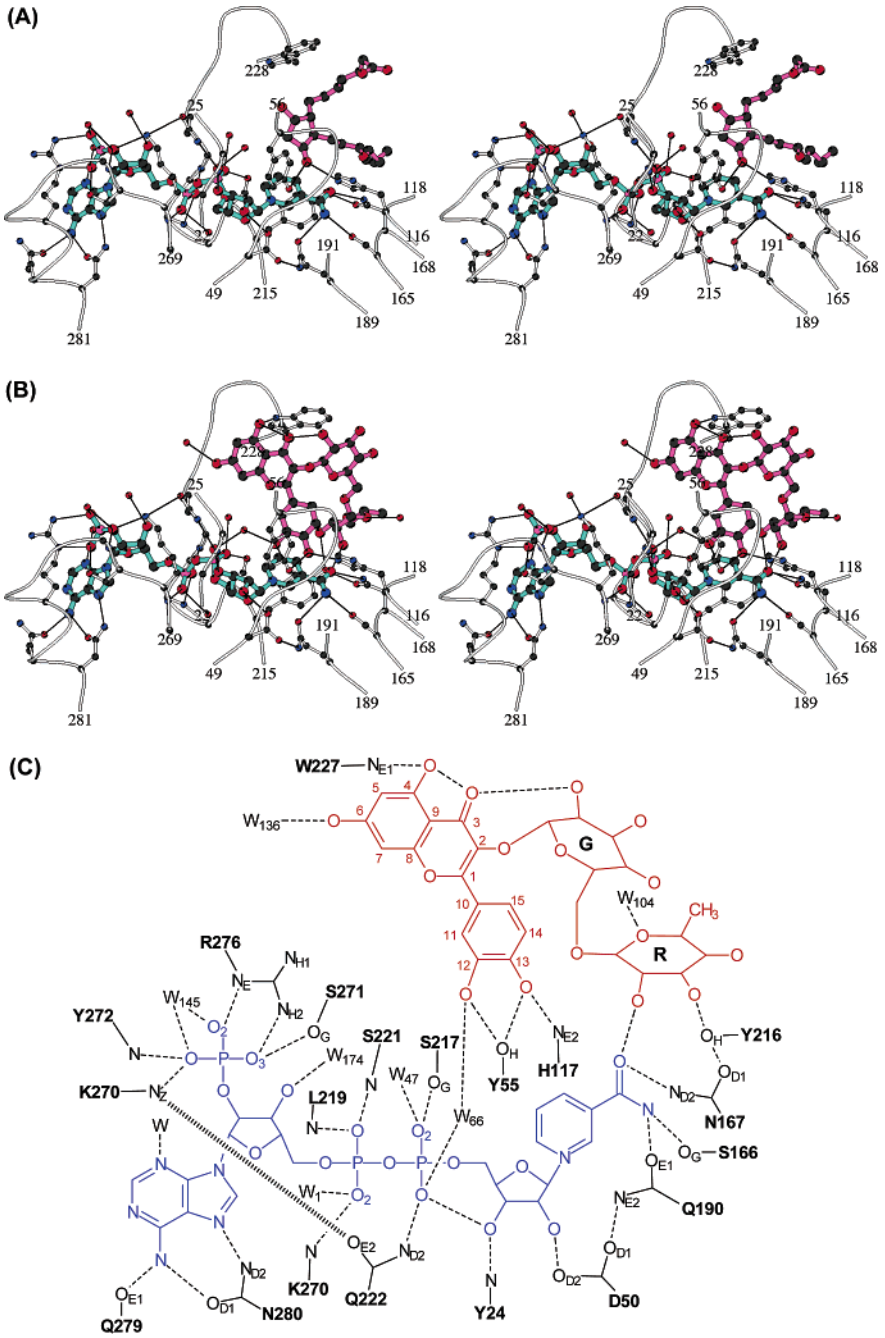

FIGURE 4: Active site geometry. Thin lines illustrate possible hydrogen bonds among $NADP^+$/NADPH (aquamarine), PGD_2/rutin (magenta), and protein (white). Loops are illustrated with coils: (A) PGFS−($NADP^+$+PGD_2) and (B) PGFS−(NADPH+rutin). (C) Schematic illustration showing possible hydrogen bonds in the active site of PGFS−(NADPH+rutin). W's represent water molecules. The thick dashed line represents a safety-belt hydrogen bond. The hydrogen bond network of PGFS−($NADP^+$+PGD_2) is the same as that of PGFS−(NADPH+rutin) except for the involvement of rutin. For PGD_2, the carbonyl O_{11} hydrogen bonds with Y55 and H117, and the other sections of the molecule are not involved in a hydrogen bond with PGFS.

amino acid residues mainly in three large loops (loop 4, loop 7, and loop 9). Rutin forms a rough "U" shape at the active site cavity. The catechol and rhamnose moieties at either tip of the U are deep within the cavity, whereas the dihydroxychromone and glucose moieties are outside the cavity and have fewer interactions with PGFS. The catechol moiety is nearly stacked on the nicotinamide ring of NADPH. As shown in Figure 5B, the hydroxyl group of the catechol O_{13} is involved in hydrogen bonds with O_H of Y55 and N_{E2} of H117 as was observed for the carbonyl O_{11} of PGD_2. The hydroxyl group O_{12} also participates in a hydrogen bond with O_H of Y55 which forms a hydrogen bond with N_Z of K84. Therefore, O_H of Y55 forms hydrogen bonds with O_{12}, O_{13}, and N_Z in a trigonal fashion. N_Z of Lys84 is also involved in trigonal hydrogen bonds with O_{D1} of D50, O of S51, and O_H of Y55. The hydroxyl groups, $O_{2'}$ and $O_{3'}$, of rhamnose are involved in hydrogen bonds with Y216 and the carbamoyl group of nicotinamide of the bound NADPH, respectively. The hydroxyl group O_4 of the quercetin moiety participates in a hydrogen bond with the indole ring of W227 in loop 7. Carbonyl O_3 is involved in the two intra-hydrogen bonds with O_4 and $O_{2'}$ of the glucose moiety.

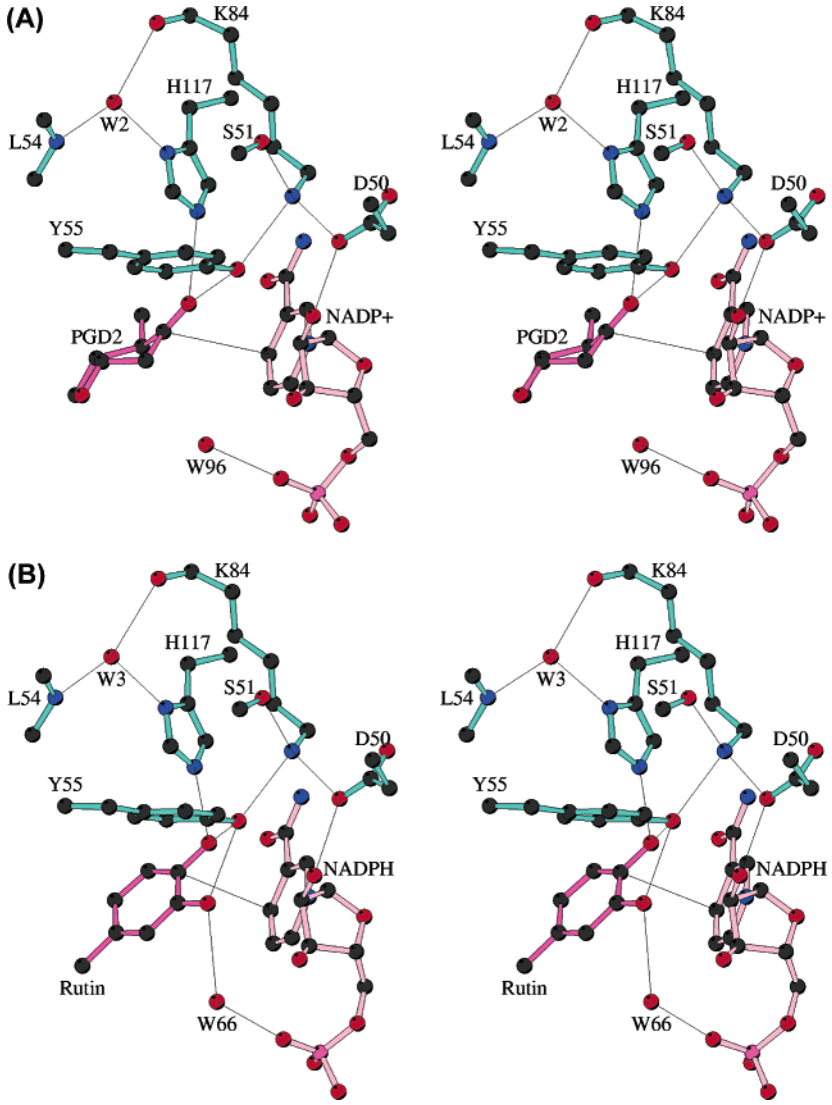

FIGURE 5: Detailed catalytic site geometry: (A) PGFS−($NADP^+$+PGD_2) and (B) PGFS−(NADPH+rutin). Portions of PGFS, $NADP^+$/NADPH, and PGD_2/rutin are colored aquamarine, light pink, and magenta, respectively.

DISCUSSION

PGSF Has a Relatively Large Active Site Cavity. Crystal structures of the PGFS−($NADP^+$+PGD_2) complex and the PGFS−(NADPH+rutin) complex have been determined in this study. Despite the significant difference between the structures of PGD_2 and rutin, the structures of PGFS in the PGFS−($NADP^+$+PGD_2) and PGFS−(NADPH+rutin) complexes are quite similar. The rmsd of C_A positions between the two structures is 0.23 Å, and all side chains are superimposable except those of W227 and F306, suggesting that the active site cavity of PGFS is relatively large so that various molecules can fit into the active site and, thus, the catalytic specificity of PGFS should be very broad. Indeed, PGFS catalyzes reduction and/or oxidation reactions of *p*-nitrobenzaldehyde, 9,10-phenanthrenequinone, phenylglyoxal, *p*-nitroacetophenone, hydrindadantin, menadione, 5β-dihydrotestosterone, 5β-androstane-3α,17β-diol, 5β-androstan-17β-ol-3-one, and 5β-androstane-3,17-dione (*14*, *23*, *24*, *53*).

PGD_2 and Rutin Are Involved in Similar Hydrogen Bonds with PGFS. As shown in Figure 6, the cyclopentane moiety of PGD_2 and the catechol moiety of rutin are roughly superimposable. O_{11} of PGD_2 and O_{13} of rutin are involved in the same hydrogen bonds with O_H of Y55 and N_{E2} of H117. However, as shown in Figure 7, the exact hydrogen bond schemes are different because O_{11} of PGD_2 is a carbonyl oxygen while O_{13} of rutin is a hydroxyl oxygen. O_H of Y55 is a hydrogen bond donor in the $OH\cdots O_{11}$ hydrogen bond and participates in two hydrogen bonds in the PGD_2 complex, while in the rutin complex, O_H is a hydrogen bond acceptor in the $OH\cdots O_{13}$ hydrogen bond and participates in three hydrogen bonds. This alternative hydrogen bonding is possible because the adjacent O_{12} hydroxyl group of the catechol moiety of rutin can be involved as a hydrogen bond acceptor of O_H of Y55. O_{12} also hydrogen bonds to a water (W_{66}), which is connected to the phosphate moiety of the nicotinamide mononucleotide by a hydrogen bond. In the PGD_2 complex, a water (W_{96}) is located at the same site and is involved in a hydrogen bond with the phosphate, but does not interact with the bound PGD_2. In addition to the catechol moiety interactions, the rhamnose moiety of the bound rutin interacts with PGFS and the bound NADPH. Rutin would be a potent inhibitor because it can bind tightly to the active site, considering the hydrogen bonding capability of rutin in the active site of PGFS. As

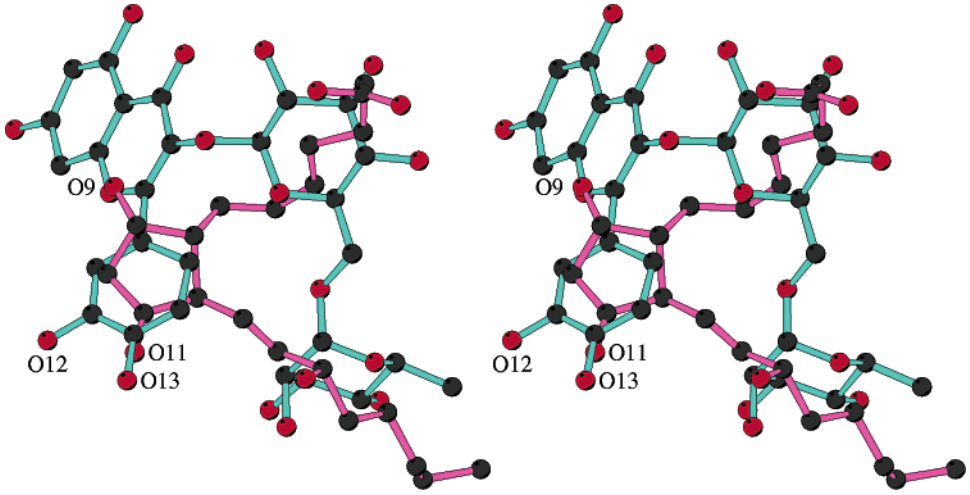

FIGURE 6: Superimposed view of the substrate (PGD_2) in the PGFS−($NADP^+$+PGD_2) structure and the inhibitor (rutin) in the PGFS−(NADPH+rutin) structure showing that the cyclopentane ring of PGD_2 and the phenyl ring of rutin approximately overlap. The two tails of PGD_2 are located over the glucose and rhamnose moieties of rutin.

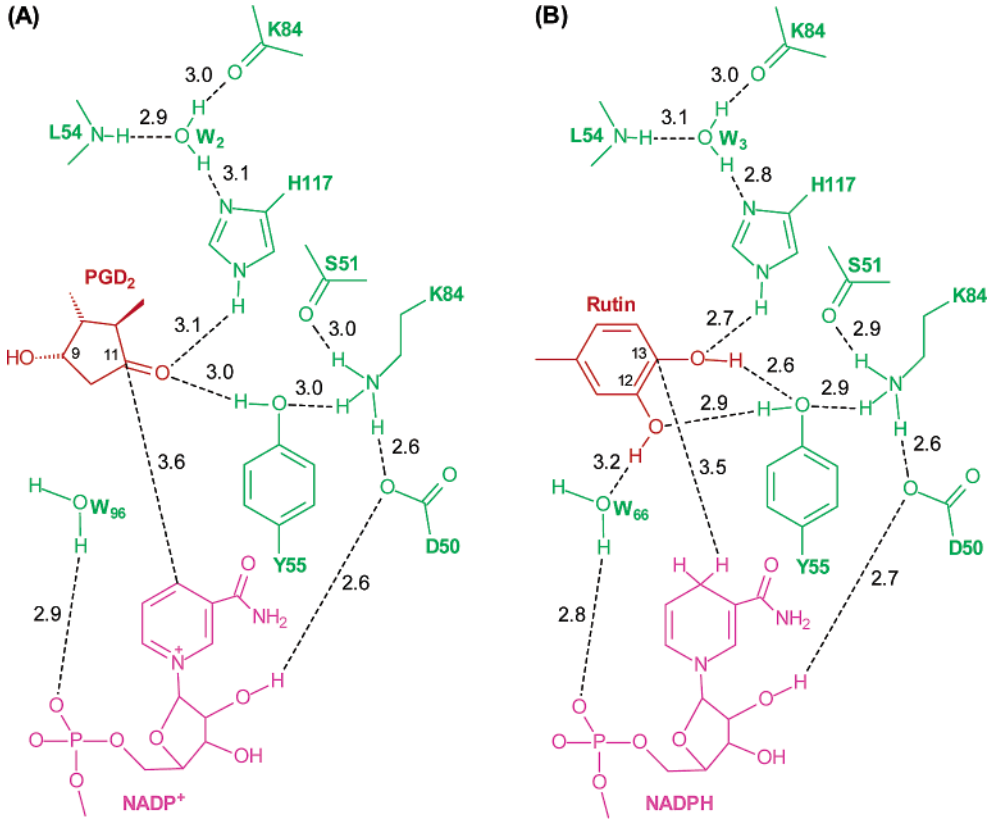

FIGURE 7: Schematic illustration showing possible hydrogen bond donors and acceptors. The numbers along the dashed lines are O···O or O···N hydrogen bond distances. Also, C_4[NADP]···C_{11}[PGD_2]/C_{13}[rutin] distances are given.

will be discussed below, when PGD_2 enters the active site, the essential section (>C_{11}=O_{11}) for the catalytic reaction binds tightly to the enzyme via two hydrogen bonds (O_{11}···O_H[Y55] and O_{11}···N_{E2}[H117]). Then, the bound PGD_2 is reduced by a direct hydride transfer from NADPH to C_{11} and protonation of O_{11}; the electron configuration of C_{11} is changed from sp^2 to sp^3, and consequently, the two hydrogen bonds (N_{E2-H}[H117]···O_{11-H}···O_H[Y55]) weaken or break because the O_{11} moves substantially. Thus, PGD_2 is a good substrate because after the catalytic reaction the product 9α,11β-PGF_2 can leave easily from the active site.

Comparison between PGFS and AKR1C1 (20α-HSD) or AKR1C2 (3α-HSD Type 3). PGFS, AKR1C1, and AKR1C2 are all composed of 323 amino acid residues. The amino acid sequences of AKR1C1 and AKR1C2 are almost identical (i.e., only seven amino acid residues are different). The amino acid sequence of AKR1C3 (PGFS) differs from that of AKR1C1 at 39 sites and that of AKR1C2 at 42 sites. As shown in Table 2, the major differences are seen in the loop sections (30 and 31 amino acid residues are different from those of AKR1C1 and AKR1C2, respectively). Nevertheless, the structure of PGFS can be superimposed on the equivalent C_A positions of AKR1C1 (*50*) and AKR1C2 (*51*, *52*) with rmsds of 0.88 and 0.75 Å, respectively (Figure 8). In particular, the $\alpha\beta$ barrel base of PGFS is nearly identical to those of AKR1C1 and AKR1C2. The amino acid residues

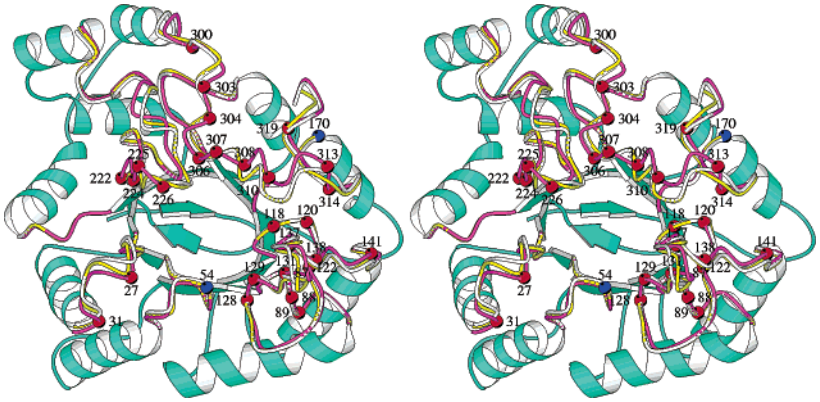

FIGURE 8: Superimposed view of PGFS, AKR1C1, and AKR1C2 showing the similarity of three AKR enzymes. The C_A atoms of AKR1C1 and AKR1C2 were superimposed on the corresponding C_A atoms of PGFS by a least-squares method. The nearly identical α/β barrel base structure is shown with ribbon drawings, while the loop sections of PGFS, AKR1C1, and AKR1C2 are depicted as magenta, white, and yellow coils, respectively. The different amino acid sites of PGFS, AKR1C1, and AKR1C2 are represented with red, black, and blue spots with the amino acid residue numbers, respectively.

Table 2: Amino Acid Sequences of Nine Loops in PGFS along with Those of AKR1C1 and AKR1C2[a]

Loop-1:	22-GTYAPPEVPRS-32
AKR1C1	GTYAPAEVPKS
AKR1C2	GTYAPAEVPKS
Loop-2:	50-DSAHLYNNE-58
AKR1C1	DSAHLYNNE
AKR1C2	DSAHVYNNE
Loop-3:	85-LWSTFHRP-92
AKR1C1	LWCNSHRP
AKR1C2	LWSNSHRP
Loop-4:	116-IHSPMSLKPGEELSPTDEDGKVIFDIVDL-144
AKR1C1	IHFPVSVKPGEEVIPKDEDGKILFDTVDL
AKR1C2	IHFPVSVKPGEEVIPKDEDGKILFDTVDL
Loop-5:	166-SNFNR-170
AKR1C1	SNFNR
AKR1C2	SNFNH
Loop-6:	192-ECHPYFNRS-200
AKR1C1	ECHPYFNQR
AKR1C2	ECHPYFNQR
Loop-7:	216-YSALGSQRDKRWVDPNSPVLLEDP-239
AKR1C1	YSALGSHREEPWVDPNSPVLLEDP
AKR1C2	YSALGSHREEPWVDPNSPVLLEDP
Loop-8:	270-KSYNE-274
AKR1C1	KSYNE
AKR1C2	KSYNE
Loop-9:	297-DGLDRNLHYFNSDSFASHPNYPYSDEY-323
AKR1C1	DGLNRNVRYLTLDIFAGPPNYPFSDEY
AKR1C2	DGLNRNVRYLTLDIFAGPPNYPFSDEY

[a] Red residues are different from the residues in the same position in the other proteins.

involved in interactions with the cofactor are also highly conserved except for residue 222. AKR1C1 and AKR1C2 have histidine at residue 222, in contrast to glutamine in PGFS. Because of steric hindrance of the imidazole ring of H222, a characteristic safety-belt hydrogen bond over the bound cofactor is lacking in the AKR1C1 and AKR1C2 structures. The bound NADP in the PGFS structure is held in place by the safety-belt hydrogen bond (N_Z[K270]$\cdots O_{E1}$-[Q222]), which is found in most members of the AKR superfamily (*54*−*56*).

The main chains of large loops 4, 7, and 9 of PGFS slightly, but significantly, deviate from those of AKR1C1−($NADP^+$+progesterone) (*50*) and AKR1C2−($NADP^+$+ursodeoxycholate) complexes (*51*). The largest deviation is observed between residues 305 and 313 in loop 9. If a rutin molecule binds to either AKR1C1 or AKR1C2, obvious collisions would occur in several sections (residues 118, 129, 222, 224, and 308). The amino acid residues of PGFS in these sections are all replaced with smaller residues (F118 → S118, I129 → S129, H222 → Q222, E224 → D224, and L308 → S308). Interestingly, if either progesterone or ursodeoxycholate binds to PGFS as observed in the structures of AKR1C1−($NADP^+$+progesterone) and AKR1C2−($NADP^+$+ursodeoxycholate) complexes (*50*, *51*), these steroids would fit well in the active site of PGFS without any critical short contacts. This is consistent with the fact that PGFS can accommodate various compounds in the active site and can catalyze reduction and/or oxidation reactions as described above. AKR1C1 and AKR1C2 have relatively narrow substrate specificities, whereas PGFS (AKR1C3) has a relatively broad substrate specificity, although the main chain structure is quite similar to those of AKR1C1 and AKR1C2. Apparently, the broad substrate specificity of PGFS is due to the mutations in the loop sections.

Proposed Catalytic Mechanism. All AKRs follow a sequential ordered bi-bi mechanism in which the cofactor binds first and leaves last (*57*). The binding and release of the cofactor are proposed to be the rate-determining steps for the overall catalysis of aldehyde and aldose reductases (*58*). In the structure of PGFS, indeed, the cofactor NADPH binds deeply in the cavity and the substrate PGD_2 is located above the cofactor, indicating that the catalytic mechanism is a sequential ordered bi-bi mechanism in which NADPH binds first. The conformational rearrangements associated with the formation and disruption of the safety belt upon cofactor binding and release are suggested to be the slowest step of the reaction (*58*).

In the crystal structures of PGFS−($NADP^+$+PGD_2) and PGFS−(NADPH+rutin), the cyclopentane ring of PGD_2 and the phenyl ring of rutin are nearly parallel to the nicotinamide

ring of NADP and face the *re*-side of the nicotinamide ring. The distances, C_4[$NADP^+$]···C_{11}[PGD_2] and C_4[NADPH]···C_{13}[rutin], are 3.6 and 3.5 Å, respectively. These geometrical features suggest that a direct hydride transfer from NADPH to PGD_2 would be a reasonable catalytic mechanism. The hydride transfer is facilitated by protonation of the carbonyl O_{11} of PGD_2 from either H117 or Y55, each of which is involved in hydrogen bonds with the carbonyl oxygen (O_{11}). As shown in Figures 5 and 7, N_{D1} of H117 is involved in a hydrogen bond with a well-defined water (W_2) in a water channel, indicating that H117 is exposed to solvent and thus the protonation or deprotonation of the imidazole ring of H117 is influenced by the pH of the environment. H117 would be protonated below pH 6, while it would be neutral above pH 7. Therefore, it would be an ideal proton donor in a slightly acidic environment.

O_H of Y55 is involved in hydrogen bond networks with K84 which is salt-linked to D50 (Figures 5 and 7). These residues, including H117, are essential for HSD catalysis and are known as the catalytic tetrad (*59*). The tetrad, which is highly conserved throughout the AKR superfamily, has an identical spatial arrangement relative to the nicotinamide ring of NADP in the complexes of AKR1C2 (*57*). Schelegel *et al*. (*59*) have determined that Y55 acts as a general acid and base in the AKR1C2 catalysis. A mutation study indicates that the Y55F mutation completely eliminates the PGD_2, PGH_2, and PQ reductase activities of PGFS (*18*). Therefore, PGFS would be able to use Y55 as the general acid to donate a proton to O_{11} of PGD_2 in a slightly basic environment. PGFS has an appreciable reduction activity ($PGD_2 \rightarrow 9\alpha,11\beta$-$PGF_2$) over a wide pH range [from pH 6 (*26*) to 9 (*27*)]. Similarly, the oxidation activity ($9\alpha,11\beta$-$PGF_2 \rightarrow PGD_2$) has been detected from pH 7.4 to 10 (*26*, *27*). These results indicate that PGFS is capable of catalyzing the reduction and oxidation reactions over a rather wide pH range, which is supported by the presence of two general acid or base residues in the catalytic site.

CONCLUSION

Human lung PGFS is human AKR1C3, and its amino acid sequence and three-dimensional structure are very similar to those of AKR1C1 and AKR1C2. However, the active site of PGFS is designed to accommodate various compounds, while those of AKR1C1 and AKR1C2 are designed to distinguish the substrates. PGFS has two possible general acid residues (H117 and Y55) which facilitate the direct hydride transfer from NADPH to PGD_2. A natural compound, rutin, can bind tightly to PGFS with polar and nonpolar interactions, and inhibits substrate binding (i.e., it is a competitive inhibitor).

ACKNOWLEDGMENT

We express our thanks to the 19BM beamline staff at APS for assistance and to Professor Richard H. Himes and Mr. Ken Takusagawa for a critical reading of the manuscript and very valuable comments.

REFERENCES

1. Johnson, M., Carey, F., and McMillan, R. M. (1983) Alternative pathways of arachidonate metabolism: prostaglandins, thromboxane and leukotrienes, *Essays Biochem. 19*, 40−141.
2. Bergström, S. (1966) in *Nobel Symposum 2, Prostaglandins* (Bergström, S., and Samuelsson, B., Eds.) pp 21−30, Almqvist and Wiksell, Stockholm.
3. Karim, S. M., Sandler, M., and Williams, E. D. (1967) Distribution of prostaglandins in human tissues, *Br. J. Pharmacol. Chemother. 31*, 340−344.
4. Embrey, M. P., and Morrison, D. L. (1968) The effect of prostaglandins on human pregnant myometrium *in vitro*, *J. Obstet. Gynaecol. Br. Commonw. 75*, 829−832.
5. Karim, S. M., Trussell, R. R., Patel, R. C., and Hillier, K. (1968) Response of pregnant human uterus to prostaglandin-F_2-α-induction of labour, *Br. Med. J. 4*, 621−623.
6. Hyman, A. L. (1969) The active responses of pulmonary veins in intact dogs to prostaglandins $F_{2\alpha}$ and E_1, *J. Pharmacol. Exp. Ther. 165*, 267−273.
7. Mathé, A. A. (1977) in *The Prostaglandins* (Ramwell, P. W., Ed.) Vol. 3, pp 169−224, Plenm, New York.
8. Watanabe, K., Shimizu, T., and Hayaishi, O. (1981) Enzymatic conversion of prostaglandin D_2 to $F_{2\alpha}$ in the rat lung, *Biochem. Int. 2*, 603−610.
9. Wong, P. Y.-K. (1981) Purification and partial characterization of prostaglandin D_2 11-keto reductase in rabbit liver, *Biochim. Biophys. Acta 659*, 169−178.
10. Leslie, C. A., and Levine, L. (1973) Evidence for the presence of a prostaglandin E 2-9-keto reductase in rat organs, *Biochem. Biophys. Res. Commun. 52*, 717−724.
11. Lin, Y.-M., and Jarabak, J. (1978) Isolation of two proteins with 9-ketoprostaglandin reductase and NADP-linked 15-hydroxyprostaglandin dehydrogenase activities and studies on their inhibition, *Biochem. Biophys. Res. Commun. 81*, 1227−1234.
12. Hamberg, M., and Samuelsson, B. (1967) On the mechanism of the biosynthesis of prostaglandins E-1 and F-1-α, *J. Biol. Chem. 242*, 5336−5343.
13. Wlodawer, P., Kindahl, H., and Hamberg, M. (1976) Biosynthesis of prostaglandin $F_{2\alpha}$ from arachidonic acid and prostaglandin endoperoxides in the uterus, *Biochim. Biophys. Acta 431*, 603−614.
14. Qureshi, Z., and Cagen, L. M. (1982) Prostaglandins $F_{2\alpha}$ produced by rabbit renal slices is not a metabolite of prostaglandins E_2, *Biochem. Biophys. Res. Commun. 104*, 1255−1263.
15. Watanabe, K., Yoshida, R., Shimizu, T., and Hayaishi, O. (1985) Enzymatic formation of prostaglandin $F_{2\alpha}$ from prostaglandin H_2 and D_2. Purification and properties of prostaglandin F synthetase from bovine lung, *J. Biol. Chem. 260*, 7035−7041.
16. Watanabe, K., Iguchi, Y., Iguchi, S., Arai, Y., Hayaishi, O., and Roberts, L. J., II (1986) Stereospecific conversion of prostaglandin D_2 to (5Z,13E)-(15S)-9α-11β,15-trihydroxyprosta-5,13-dien-1-oic acid ($9\alpha,11\beta$-prostaglandin F_2) and of prostaglandin H_2 to prostaglandin $F_{2\alpha}$ by bovine lung prostaglandin F synthase, *Proc. Natl. Acad. Sci. U.S.A. 83*, 1583−1587.
17. Watanabe, K., Fujii, Y., Nakayama, K., Ohkubo, H., Kuramitsu, S., Kagamiyama, H., Nakanishi, S., and Hayaishi, O. (1988) Structural Similarity of Bovine Lung Prostaglandin F Synthase with ϵ-Crystallin of European Common Frog, *Proc. Natl. Acad. Sci. U.S.A. 85*, 11−15.
18. Suzuki, K., Fujii, Y., Miyano, M., Chen, L.-Y., Takahashi, T., and Watanabe, K. (1999) cDNA Cloning, Expression, and Mutagenesis Study of Liver-type Prostaglandin F Synthase, *J. Biol. Chem. 274*, 241−248.
19. Hara, A., Taniguchi, H., Nakayama, T., and Sawada, H. (1990) Purification and properties of multiple forms of dihydrodiol dehydrogenase from human liver, *J. Biochem. 108*, 250−254.
20. Takikawa, H., Fujimoto, M., Nishikawa, K., and Yamada, M. (1992) Purification of 3α-hydroxysteroid and 3β-hydroxysteroid dehydrogenases from human liver cytosol, *Hepatology 16*, 365−371.
21. Qin, K.-N., New, M. I., and Cheng, K.-C. (1995) Molecular cloning of multiple cDNAs encoding human enzymes structurally related to 3α-hydroxysteroid dehydrogenase, *J. Steroid Biochem. Mol. Biol. 46*, 673−679.
22. Stolz, A., Hammond, L., Lou, H., Takikawa, H., Ronk, M., and Shively, J. E. (1993) cDNA cloning and expression of the human hepatic bile-acid-binding protein. A member of the monomeric reductase gene family, *J. Biol. Chem. 268*, 10448−10457.
23. Deyashiki, Y., Ogasawara, A., Nakayama, T., Nakanishi, M., Miyabe, Y., and Hara, A. (1994) Molecular cloning of two human liver 3α-hydroxysteroid/dihydrodiol dehydrogenase isoenzymes that are identical with chlordecone reductase and bile-acid binder, *Biochem. J. 299*, 545−552.

24. Khanna, M., Qin, K.-N., Wang, R. W., and Cheng, K.-C. (1995) Substrate specificity, gene structure, and tissue-specific distribution of multiple human 3α-hydroxysteroid dehydrogenase, *J. Biol. Chem. 270*, 20162−20168.
25. Jez, J. M., Flynn, T. G., and Penning, T. M. (1997) A new nomenclature for the aldo-keto reductase superfamily, *Biochem. Pharmacol. 54*, 639−647.
26. Matsuura, K., Shiraishi, H., Hara, A., Sato, K., Deyashiki, Y., Ninomiya, M., and Sakai, S. (1998) Identification of a principle mRNA species for human 3α-hydroxysteroid dehydrogenase isoform (AKR1C3) that exhibits high prostaglandin D_2 11-ketoreductase activity, *J. Biochem. 124*, 940−946.
27. Suzuki-Yamamoto, T., Nishizawa, M., Fukui, M., Okuda-Ashitaka, E., Nakajima, T., Ito, S., and Watanabe, K. (1999) cDNA cloning, expression and characterization of human prostaglandin F synthase, *FEBS Lett. 462*, 335−340.
28. Mammalian Gene Collection Program Team (Strausberg, R. L., *et al*.) (2002) Generation and initial analysis of more than 15,000 full-length human and mouse cDNA sequences, *Proc. Natl. Acad. Sci. U.S.A. 99*, 16899−16903.
29. Liston, T. E., and Roberts, L. J., II (1985) Transformation of prostaglandin D_2 to 9α,11β-(15S)-trihydroxyprosta-(5Z,13E)-dien-1-oic acid (9α,11β-prostaglandin F_2): a unique biologically active prostaglandin produced enzymatically *in vivo* in humans, *Proc. Natl. Acad. Sci. U.S.A. 82*, 6030−6034.
30. Pugliese, G., Spokas, E. G., Marcinkiewicz, E., and Wong, P. Y.-K. (1985) Hepatic transformation of prostaglandin D_2 to a new prostanoid, 9α,11β-prostaglandin F_2, that inhibits platelet aggregation and constricts blood vessels, *J. Biol. Chem. 260*, 14621−14625.
31. Beasley, C. R., Robinson, C., Featherstone, R. L., Varley, J. G., Hardy, C. C., Church, M. K., and Holgate, S. T. (1987) 9α,11β-Prostaglandin F_2, a novel metabolite of prostaglandin D_2 is a potent contractile agonist of human and guinea pig airways, *J. Clin. Invest. 79*, 978−983.
32. Seibert, K., Sheller, J. R., and Roberts, L. J., II (1987) (5Z,13E)-(15S)-9α,11β,15-Trihydroxyprosta-5,13-dien-1-oic acid (9α,11β-prostaglandin F_2): formation and metabolism by human lung and contractile effects on human bronchial smooth muscle, *Proc. Natl. Acad. Sci. U.S.A. 84*, 256−260.
33. Dworski, R., Fitzgerald, G. A., Oates, J. A., and Sheller, J. R. (1994) Effect of oral prednisone on airway inflammatory mediators in atopic asthma, *Am. J. Respir. Crit. Care Med. 149*, 953−959.
34. Obata, T., Nagakura, T., Kammuri, M., Masaki, T., Maekawa, K., and Yamashita, K. (1994) Determination of 9α,11β-prostaglandin F_2 in human urine and plasma by gas chromatography−mass spectrometry, *J. Chromatogr., B: Biomed. Sci. Appl. 655*, 173−178.
35. O'Sullivan, S., Dahlén, B., Dahlén, S. E., and Kumlin, M. (1996) Increased urinary excretion of the prostaglandin D_2 metabolite 9α,-11β-prostaglandin F_2 after aspirin challenge supports mast cell activation in aspirin-induced airway obstruction, *J. Allergy Clin. Immunol. 98*, 421−432.
36. Griffith, J. Q., Couch, J. F., and Lindauer, A. (1944) Effect of rutin on increased capillary fragility in man, *Proc. Soc. Exp. Biol. Med. 55*, 228−229.
37. Schilcher, H., Patz, B., and Schimmel, K. (1990) Ch. Klinische Studie mit einerm Phytopharmakon zur Behandlung von Mikrozirkulatiönsstorungen, *Ärztezeitschrift Naturheilverfahren 31*, 819−826.
38. Wojcicki, J., Barcew-Wiszniewska, B., Samochowiec, L., and Rozewicka, L. (1995) Extractum Fagopyri reduces atherosclerosis in high-fat diet fed rabbits, *Pharmazie 50*, 560−562.
39. Watanabe, M. (1998) Catechins as antioxidants from buckwheat (*Fagopyrum esculentum* Moench) groats, *J. Agric. Food Chem. 46*, 839−845.
40. Wilhelm, K. P., Biel, S., and Siegers, C. P. (2001) Role of flavonoids in controlling the phototoxicity of *Hypericum perforatum* extracts, *Phytomedicine 8*, 306−309.
41. Arima, H., Ashida, H., and Danno, G. (2002) Rutin-enhanced antibacterial activities of flavonoids against *Bacillus cereus* and*Salmonella enteritidis*, *Biosci., Biotechnol., Biochem. 66*, 1009−1014.
42. Sawada, H., and Hara, A. (1979) The presence of two NADPH-linked aromatic aldehyde-ketone reductases different from aldehyde reductase in rabbit liver, *Biochem. Pharmacol. 28*, 1089−1094.
43. Sawada, H., Hara, A., Kato, F., and Nakayama, T. (1979) Purification and properties of reductases for aromatic aldehydes and ketones from guinea pig liver, *J. Biochem. 86*, 871−881.
44. Ahmed, N. K., Felsted, R. L., and Bachur, N. R. (1979) Comparison and characterization of mammalian xenobiotic ketone reductases, *J. Pharmacol. Exp. Ther. 209*, 12−19.
45. Chen, L.-Y., Watanabe, K., and Hayaishi, O. (1992) Purification and characterization of prostaglandin F synthase from bovine liver, *Arch. Biochem. Biophys. 296*, 17−26.
46. Otwinowski, Z., and Minor, W. (1997) Processing of X-ray diffraction data collected in oscillation mode, *Methods Enzymol. 276*, 307−326.
47. Brünger, A. T. (1993) *X-PLOR 3.82: A system for X-ray crystallography and NMR*, Yale University Press, New Haven, CT.
48. Laskowski, R. A., MacArthur, M. W., Moss, D. S., and Thornton, J. M. (1993) ROCHECK: A program to check the stereochemical quality of protein structures, *J. Appl. Crystallogr. 26*, 283−291.
49. Jez, J. M., Bennett, M. J., Schlegel, B. P., Lewis, M., and Penning, T. M. (1997) Comparative anatomy of the aldo-keto reductase superfamily, *Biochem. J. 326*, 625−636.
50. Couture, J. F., Legrand, P., Cantin, L., Luu-The, V., Labrie, F., and Breton, R. (2003) Human 20α-hydroxysteroid dehydrogenase: crystallographic and site-directed mutagenesis studies lead to the identification of an alternative binding site for C21-steroids, *J. Mol. Biol. 331*, 593−604.
51. Jin, Y., Stayrook, S. E., Albert, R. H., Palackal, N. T., Penning, T. M., and Lewis, M. (2001) Crystal structure of human type III 3α-hydroxysteroid dehydrogenase/bile acid binding protein complexed with $NADP^+$ and ursodeoxycholate, *Biochemistry 40*, 10161−10168.
52. Nahoum, V., Gangloff, A., Legrand, P., Zhu, D. W., Cantin, L., Zhorov, B. S., Luu-The, V., Labrie, F., Breton, R., and Lin, S. X. (2001) Structure of the human 3α-hydroxysteroid dehydrogenase type 3 in complex with testosterone and NADP at 1.25 Å resolution, *J. Biol. Chem. 276*, 42091−42098.
53. Nishizawa, M., Nakajima, T., Yasuda, K., Kanzaki, H., Sasaguri, Y., Watanabe, K., and Ito, S. (2000) Close Kinship of Human 20α-Hydroxysteroid Dehydrogenase Gene with Three Aldo-keto Reductase Genes, *Genes Cells 5*, 111−125.
54. Wilson, D. K., Bohren, K. M., Gabbay, K. H., and Quiocho, F. A. (1992) An unlikely sugar substrate site in the 1.65 Å structure of the human aldose reductase holoenzyme implicated in diabetic complications, *Science 257*, 81−84.
55. Borhani, D. W., Harter, T. M., and Petrash, J. M. (1992) The crystal structure of the aldose reductase·NADPH binary complex, *J. Biol. Chem. 267*, 24841−24847.
56. el-Kabbani, O., Judge, K., Ginell, S. L., Myles, D. A., DeLucas, L. J., and Flynn, T. G. (1995) Structure of porcine aldehyde reductase holoenzyme, *Nat. Struct. Biol. 2*, 687−692.
57. Penning, T. M. (1999) Molecular determinants of steroid recognition and catalysis in aldo-keto reductases. Lessons from 3α-hydroxysteroid dehydrogenase, *J. Steroid Biochem. Mol. Biol. 69*, 211−225.
58. Grimshaw, C. E., Bohren, K. M., Lai, C. J., and Gabbay, K. H. (1995) Human aldose reductase: rate constants for a mechanism including interconversion of ternary complexes by recombinant wild-type enzyme, *Biochemistry 34*, 14356−14365.
59. Schlegel, B. P., Jez, J. M., and Penning, T. M. (1998) Mutagenesis of 3 α-hydroxysteroid dehydrogenase reveals a "push-pull" mechanism for proton transfer in aldo-keto reductases, *Biochemistry 37*, 3538−3548.

BI036046X